Two-phase flow in a rough fracture: Experiment and modeling

M. Ferer,[1,2] Dustin Crandall,[3,4] Goodarz Ahmadi,[4] and Duane H. Smith[1,2]
[1]*US DOE, National Energy Technology Laboratory, Morgantown, West Virginia 26507-0880, USA*
[2]*Physics Department, West Virginia University, P. O. Box 6315, Morgantown, West Virginia 26506-6315, USA*
[3]*URS, Washington Division, Morgantown, West Virginia 26507-0880, USA*
[4]*Mechanical and Aeronautical Engineering Department, Clarkson University, Potsdam, New York 13699-5725, USA*
(Received 8 February 2011; revised manuscript received 20 June 2011; published 28 July 2011)

To develop and test theory-based procedures for modeling two-phase flow through fractures, it is important to be able to compare computational results for a fracture with experiments performed on the exact same fracture. Unfortunately for real fractures, any attempt to image the fracture and to produce a numerical model of the fracture accessible to computer modeling unavoidably results in a coarsening of the resolution, with the very small-scale features of the imaged fracture averaged to produce the numerical representation used in modeling. Contrary to the hope that these high-resolution features would be unimportant, several modeling efforts have shown that such changes in resolution do affect the flow. Therefore, the numerical representation is different from the real fracture because of this unavoidable coarsening of the resolution. To remove the problems caused by the use of different fractures in the experiment and in the model, the fracture used in our experiments was stereographically constructed from the same numerical representation used in the modeling so that the only difference between the experimental "fracture" and the modeling "fracture" is a manufacturing error of approximately 3% or less in the aperture sizes of the manufactured experimental model. Using several models not unlike others in the literature, we modeled injection of air into the water-saturated fracture. The modeling results are compared to experimental results for injection of air into the water-saturated stereolithographically constructed fracture. A comparison between modeling and experimental results for the essentially identical fractures shows a much better detailed agreement than obtained in other studies, which compared experimental flows on the real fracture with modeling results for a lower resolution representation of the real fracture. This suggests that many of the differences between experiment and modeling in previous work resulted from the differences between the experimental and modeling fractures. For our low capillary-number cases, the best agreement with experiment is for a modification of invasion percolation with trapping (IPwt) that included approximations to viscosity ratio effects and to the interfacial tension effects in reducing very short-range curvature.

DOI: 10.1103/PhysRevE.84.016316 PACS number(s): 47.55.dr, 47.56.+r, 47.55.N−

I. INTRODUCTION

Understanding the fluid flow through rock fractures is important for (i) predicting CO_2 transport during geologic sequestration within fractured rocks, (ii) describing methane and brine transport in fractured gas reservoirs, (iii) estimating transport distances of radioactive material from proposed nuclear storage facilities, (iv) determining contaminated zones due to contaminant transport from the spill location, and (v) evaluating the effectiveness of various enhanced oil recovery methods, as well as other technologies [1]. To better understand fluid flow through these important underground fluid pathways, several groups have developed efficient models of flow in single rough-walled fractures. A percolation-type model was used by Pyrak-Nolte *et al*. [2] to identify channels of preferential fluid motion through rough-walled fractures. This and similar single-phase flow models [3–5] have been used to show that the varying aperture of fractures in natural rocks affects the fluid transport by channeling the majority of fluid through the most open regions of the fracture. Many recent studies have focused on the way in which this channeling affects the transport of multiple fluids simultaneously through the complex geometries of natural rock fractures [6–13].

Several studies produced high-resolution computed tomography (CT) images of real fractures that yielded a voxel-by-voxel numerical value of the aperture distribution [14–16]. We will review the results of single-phase and two-phase flow experiments and modeling that were performed for these fractures [6–9,11,12,15–17].

Two obvious concerns about the simulations are the reliability of the modeling and the lower resolution averaging of the roughness of the real fracture. The imaging process is the first reduction in the resolution of the fracture. As an example, several modeling studies discussed use the recent CT image of a 101.4 mm × 25.4 mm fracture surface that the imaging process covers by approximately 3714 × 930 27.3 μm × 27.3 μm covering squares [11–13,16]. Even this reduced resolution of the imaging often exceeds memory and time constraints for the computational models. Therefore, the simulations usually further lower the resolution by averaging the aperture over a number of the covering squares from the imaging process. Therefore, the fracture used in the modeling is unavoidably different from the real fracture. Two modeling studies have specifically addressed this issue. In modeling primary imbibition in the fracture imaged by Keller, Hughes, and Blunt use a modified pore-level model, which approximately includes the effect of surface tension in smoothing the in-plane curvature of the interface [7,8,14]. They found observable differences in the flow as they progressed in four steps from the finest scale, 0.5 mm × 0.5 mm covering squares to 4 mm × 4 mm covering squares [7,8]. Using computational fluid dynamics to model single-phase flow in the fracture imaged by Karpyn *et al*., Crandall *et al*.

study the effect of increasing the size of the covering squares in six steps from $(0.49\ \text{mm})^2$ to $(0.88\ \text{mm})^2$ [5,16]. They found a marked change in the permeability and in the tortuosity of the highest-velocity paths through the fracture. These studies indicate that reducing the resolution from the physical fracture to the resolution required for practical computing does produce effectively different fractures with different flow properties. However, they do observe smaller differences between the higher resolutions [7,8].

Kim *et al*. performed a single-phase flow experiment through a fracture as well as lattice Boltzmann simulations on a numerical realization of this fracture [15]. This yielded results for the permeability in good agreement with experiment. Using the fracture imaged by Kim, Prodanović, and Bryant used a level-set method to quasi-statically model two-phase flow in this fracture as well as in two- and three-dimensional "fractured bead packs" [10,15]. Glass *et al*. developed a modified invasion percolation model (MIP), which included an averaged local in-plane curvature [6]. They created a "rough fracture" by placing two pieces of commercially textured glass plates in a transparent test cell and imbibed water into the "fracture." To determine an aperture field for their simulations, they used transmitted light imaging to measure the aperture field. In general, there is qualitative agreement between modeling occupation and the experiment; but there are real differences in the details of the imbibed water occupation. It is not clear if these differences arise from the scale coarsening used to create the "mathematical" fracture model for the MIP simulations or if they arise from defects in the MIP simulations.

In addition to performing the CT imaging of a real fracture, Karpyn *et al*. imaged the results of a series of flow experiments, including the injection of oil into the water-saturated fracture and the subsequent injection of water [11,12]. Piri and Karpyn developed a network model to predict (i) primary drainage (injection of oil into a water-saturated fracture) and (ii) imbibition (injection of water subsequent to primary drainage) [11,12]. The results from their simulations show good qualitative agreement with the previously mentioned experimental distribution of fluids within the fracture geometry [12]. Petchsingto and Karpyn used the MIP model of Glass and co-workers to model the flow in this same fracture [13]. However, as with the work of the other comparisons, there are real differences in the detailed occupation between modeling and experiment [19]. Again, it is not clear if these differences arise primarily from the scale coarsening used to create the mathematical fracture model for the simulations or if they arise from defects in the simulations.

In this paper we compare results from several efficient flow models with previously presented experimental results for injection of air into a water-saturated, translucent bench-top fracture model [12]. To within manufacturing tolerances the physical model has the exact same geometry as the fracture used in our modeling. The fracture was coarsened from the CT images of the same Berea sandstone fracture modeled by others [11–13,20]. This scale-coarsened fracture was used in both the experiments and the modeling. The computational models include: (i) a modified version of our standard pore-level model [18,21]; (ii) a standard model of invasion percolation with trapping (IPwt), (iii) a modified IPwt model (MIPwt) comparable to that of Glass and co-workers, and (iv) a further modification of MIPwt to mimic the effect of viscosity differences. Therefore, the modeling and experiments have used essentially the same fracture; the only difference involves errors in the aperture size of approximately 3% or less in the construction of the experimental flow cell.

II. EXPERIMENTS

The simulations of the next section were motivated by the experiments discussed below. The results of these simulations will be compared to the resulting experimental flow patterns. The original fracture was created by Karpyn *et al*. [16] through a 101.4 mm long, 25.4 mm diameter core of Berea sandstone. This fracture was CT scanned and used to generate the models for this study. Prior to fracturing, the core of sandstone had an 18% porosity and a permeability of 200 mD. Details of the fracture production and CT scanning can be found in Karpyn *et al*. [16] and Karpyn and Piri [11]. The original fracture was scanned with a voxel size of 27.3 μm × 27.3 μm × 32.5 μm; the 27.3 μm × 27.3 μm covering squares are at a larger scale than many details of the physical fracture. This relatively fine resolution was further coarsened to 240 μm covering squares to reduce the amount of data, thereby facilitating data transfer use on standard desktop computers and construction of the experimental model. Therefore, all distances in this paper are in units of the block size of 240 μm. This whole process of reducing the resolution of the physical fracture averages over smaller scale details of the physical fracture. Therefore, the resulting mathematical model of the real fracture has less roughness than the physical fracture. That is, in setting the aperture value of any covering square, small-scale features of the physical fracture inside this area have been averaged. Therefore, one might expect differences between simulations of flow in the model fracture and actual flow in the real fracture, as shown by some modeling studies [5,7,8].

To create an experimental model that closely mimics the aperture sizes of the scale-coarsened fracture geometry illustrated by Fig. 1, the irregular surface on one side of the fracture was converted to a plane (as in Fig. 2). Then the opposing surface was modified so that the local fracture aperture sizes remained unchanged as in Fig. 2. Having a flat upper surface prevented misalignment, thereby assuring a more accurate array of aperture sizes. The purpose of this work is to show that results from simple existing modeling efforts

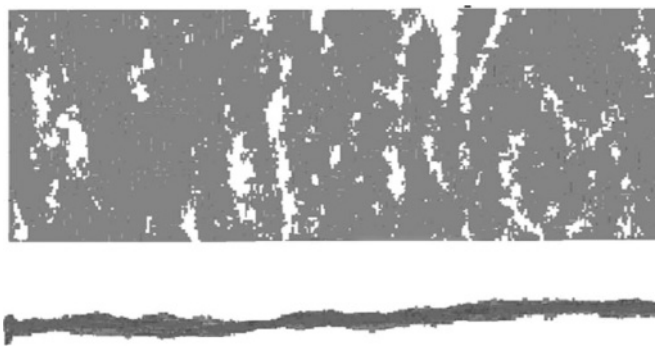

FIG. 1. CT derived fracture geometry used to create the flow models. White zones are regions of no-flow, where the fracture walls touch.

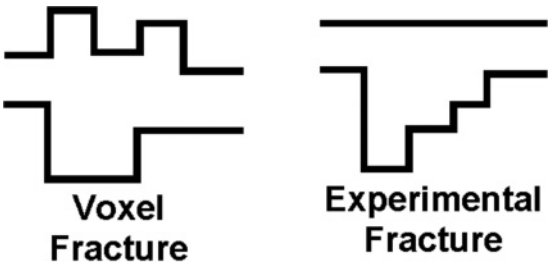

FIG. 2. Illustration of conversion of the CT voxel data to the experimental model.

agree well with experiments for a complex fracture. Therefore, for the purposes of this work, it makes little difference whether the experimental fracture mimics the right or left side of Fig. 2. It should also be noted that the modeling described in latter sections uses only the aperture size so that the modeling does not distinguish between the two illustrations in Fig. 2. The procedure shown in Fig. 2 enabled the production of a physical model using stereolithography. This is a rapid prototyping method, similar to three-dimensional (3D) printing techniques, where physical entities are created by curing a layer of photosensitive resin on the surface of a vat of heated liquid resin with a laser. A moveable platform then submerges the cured layer and an additional layer is cured on top of the previous one. This process is repeated, allowing the production of complex three-dimensional objects from computer-generated models supplied to the stereolithography apparatus. The top surface of the fracture model was flattened so that a reliable aperture distribution would be less complicated to construct using the top-down, layer-by-layer construction of stereolithography. Some details of the techniques used to create this model are presented below, additional details can be found in Crandall's thesis [20]. The final experimental model of the fracture captures the complex geometry of the coarsened-scale fracture and is translucent, which enables the direct imaging of fluid flow within the model.

This experimental fracture model was constructed with a 3D Systems Viper Si^2 SL Apparatus at Clarkson University. The stereolithography resin was a semitransparent, water-resistant, photoreactive resin, DSM 11120 Watershed (DSM Somos, New Castle DE). The bottom half of the model (with the rough fracture surface, e.g., Fig. 2) was constructed directly on a 3 in. by 6 in. by 0.25 in. plate of tempered glass. This fracture aperture distribution was centered on the glass, with a 0.5 in. of resin added along the length. Air inlet and water exit manifolds were constructed at both ends of the fracture, as shown in Fig. 3, so that the fluid pressure would be as uniform as possible along the inlet and similarly along the outlet. A higher resolution inset of the rough walled aperture is shown in Fig. 3, to illustrate the complexity of the rough fracture walls. The apertures within this model ranged from 0 to 1.92 mm, with the most-probable aperture (≈30%) being 0.48 mm [20]. The top half of the model was created from another plate of tempered glass, upon which a 0.125 in. coat of resin was cured. The halves were combined by spreading a small amount of liquid resin on the cured resin surrounding the fracture and manifolds, clamping the model halves together, and curing the model for an additional 30 min under UV light. Injection and

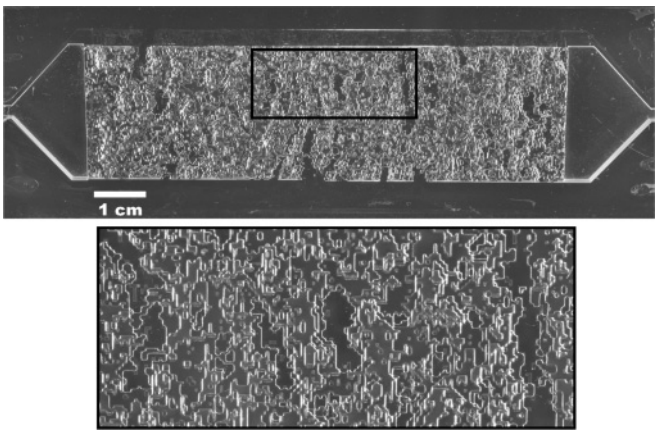

FIG. 3. Experimental stereolithography fracture model. The inset is enlarged to show the complexity of the model.

drainage tubing was then inserted into the manifolds and a quick-setting epoxy was added to the perimeter of the model to ensure stability during the experiments.

For all experiments the fracture model was horizontal to minimize gravitational effects and air was injected at a constant rate into the model initially saturated with water. The experimental setup included a constant-rate syringe pump (KD Scientific KDS 200) used to control the injection of air and a CCD camera (NTSC COHU 4915-400/000). The acquisition and storage of the images were controlled by a LabView™ module on a desktop computer. This experimental setup is shown in Fig. 4.

The ratio of the viscous forces to the interfacial forces within the fracture determine the experimental capillary-number $N_{C\text{expt}}$. Immiscible flows through rock fractures and geological porous media are often dominated by capillary forces [12]. When the capillary forces are dominant, the interfacial forces between fluids dictate the path of fluid motion by restricting motion into small cavities and pores. The capillary-number $N_{C\text{expt}}$ was calculated using

$$N_{C\text{expt}} = \frac{Q\mu}{\sigma A}. \tag{1}$$

Here A is the average cross-sectional area of the fracture perpendicular to the flow, $A = 0.74\ \text{cm}^2$; the interfacial tension σ between air and water is approximately 0.072 N/m [22];

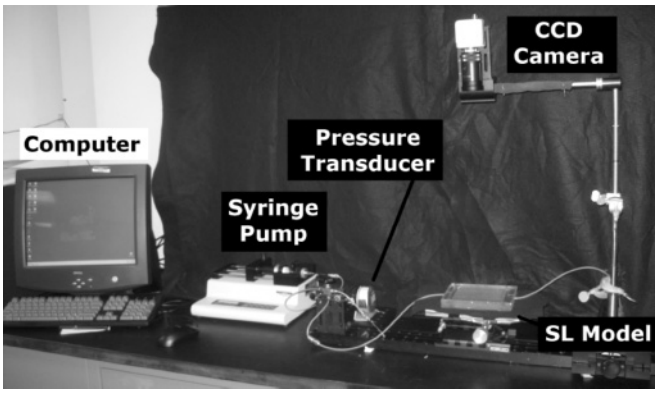

FIG. 4. Experimental setup.

FIG. 5. Experimental pattern injection from right to left. The air occupation is shown in black.

and the viscosity of water at atmospheric conditions is, $\mu = 1.8 \times 10^{-5}$ kg/(m s). These values were used in the calculation of $N_{C\text{expt}}$. For the small capillary numbers discussed in this paper, volume flows ranged from $Q = 1$ to 0.01 ml/min with capillary numbers ranging from $N_{C\text{expt}} = 5.63 \times 10^{-8}$ to 5.63×10^{-10}. At these small capillary numbers, all the experimental flows in the paper were dominated by the interfacial forces. At least three experiments were conducted at each of the velocities. For this set of experiments, there were small differences between each of the experiments, that is, there would be small differences in the air-filled fingers, which is typical of the sensitivity of low capillary number flows to small changes from one experiment to the next.

By imaging the invading, nonwetting air within the fracture we were able to measure the saturations of the two fluids during injection. For the set of experiments with flow velocity, $Q = 0.1$ ml/min, Fig. 5 shows a typical binary image of air (black) after it has traversed from right to left through the physical fracture model, initially filled with water. The path that the air followed was tortuous because of the capillary restrictions created by the small aperture regions resulting in limited connectivity of the larger aperture zones. For this set of experiments, the air occupied an average of 0.65 ml of the 1.214 ml volume of the fracture for an average air saturation of 53.5% [20].

Not surprisingly, different flow patterns were observed when fluid was injected into the two different ends of the fracture. Previous work by Crandall [20] has shown that the shape of the invading air structure (as characterized by the fractal dimension) and the saturation of air within the fracture were similar regardless of flow direction.

III. NETWORK MODELING

To study flow in porous media, we had developed a code for our standard network model (NETfLow), which includes capillary and viscous forces. This model consists of spherical pores at the sites of a diamond lattice; these pores are connected by cylindrical throats of randomly chosen cross-sectional area. The model relates the flow velocity through a throat to the pressure drop across the throat modified by any capillary pressure. Conserving volume of our incompressible fluids, a modified Gauss-Seidel iteration is performed to find the pressure field and the resulting flow velocities. The fluids are then advanced in the porous medium using flow rules that we have tried to make as nonrestrictive as possible. Although our model has many features in common with other network models in the literature [23,24], there are specific differences, which are detailed in our earlier references [25,26]. The model has also been shown to produce detailed results in agreement with experiment [18,27]. In modifying our NETfLow code to more closely mimic the flow in the fracture, we changed the transmissivity of the throats from a cylindrical to a parallel plate expression where we used the known aperture values in the parallel plate transmissivities. Since each throat represents a 3×3 covering square, the "throats" were given a much larger area than the pore bodies at the corners of the 3×3 covering square. The capillary pressure in each 3×3 covering square was taken to depend inversely only upon the aperture value. In this model, we neglected in-plane smoothing of the interface by the interfacial tension.

In Piri and Karpyn's network modeling of primary drainage, comparison of experimental and modeling flow patterns for $S_w \approx 0.35$ [Figs. 3(a) and 3(b)–3(e)] show good qualitative agreement with a number of similarities. However, there are also real differences in the patterns. These may be due to the differences between the real fracture and the numerical model of the fracture since the experiments are performed on the real fracture while the modeling is performed on the lower resolution numerical model [12]. Notably, the experimental patterns tend to show more compact (i.e., less ramified) occupation by the injected oil than does the modeling. It should be noted that in their figures the flow is from left to right. These authors also compare modeling results with experimental results for imbibition {Figs. 12(b)–12(d) in Ref. [12]} and for secondary drainage {Figs. 14(a) and 14(b) also in Ref. [12]}. Again, for all these cases, there is good qualitative agreement between the modeling and experimental results, but there are also real differences between the two. For secondary drainage {Figs. 14(a) and 14(b) in Ref. [12]} the experimental oil occupation is more compact, as it was for the primary drainage [12]. Therefore, although this efficient network modeling approach does provide real insight into the two-phase flow in a rough fracture, details of the occupation by the two fluid phases from modeling exhibit real differences with experiment.

Similar to Piri and Karpyn, we have modified our standard network model (NETfLow) [21] to study two-phase flow in a fracture with correct viscosity ratio and capillary number. From the construction of the experimental flow cell, discussed in the previous section, we know the aperture w of each covering square. Unfortunately, because of computer run-time considerations, the resolution of the model for the network simulations was further reduced so that each covering square in the computer model consisted of 3×3 covering squares in the experimental model. Therefore, the aperture of each covering square in the computer model is the average of nine apertures in the experimental model. Even with this reduced resolution, our program takes more than a month to run on a fast desktop computer. In this network modeling, we mimicked the experiment as closely as possible by using the same viscosity ratio and a capillary number in the capillary dominated regime. Figure 6 shows the overlay of our network modeling pattern on top of the experimental pattern for primary drainage shown in Fig. 5.

This clearly mimics many of the details of the flow, especially near the inlet; but fails in reproducing some of the more torturous flow paths near the middle of the fracture. The reduced resolution of the fracture aperture data in the center

FIG. 6. The occupation of air in the experimental cell is shown by the solid black flow pattern (Fig. 5). The air occupation from the network modeling is shown by the gray 3 × 3 squares. Again, flow of the injected air is from right to left.

of the numerical model likely smoothes over some restrictive regions that may hinder the flow through the center of the cell, causing the flow pattern to be less tortuous. The air occupation from network modeling is also significantly less compact than the experimental result and produces fingers not in the experimental pattern, which may be partly due to our neglect of the in-plane smoothing of the interface by the interfacial tension. However, this detailed agreement is surprisingly good given the reduced resolution of the numerical model and the neglect of the smoothing of the in-plane interface due to interfacial tension. It should be noted that this is the only "efficient" method of modeling two-phase flow in a rough fracture that is general enough to incorporate the effects of capillary number, viscosity ratio, and gravity.

A. Modifications of invasion percolation

1. Including the role of interfacial tension in reducing interfacial curvature

By itself, invasion percolation with trapping (IPwt) is significantly more efficient than the network model [28]. In IPwt that covering square with the largest aperture, adjacent to the interface, is invaded. Using the same covering squares as in the experimental model, this model network is essentially identical to the experimental network and it required only a few minutes of computer time on a laptop. The results of the IPwt model is shown in Fig. 7, where the experimental air occupation is shown in gray, while the air occupation from modeling is shown by black pixels. When compared with the network model results, this fine-scale IPwt provides more realistic results near the middle of the pattern, but again it produces a number of additional fingers and is much less compact than the result from experiment.

The effect of interfacial tension in smoothing the in-plane curvature would make the modeling pattern in Fig. 7 more compact with smoother boundaries, which should bring these

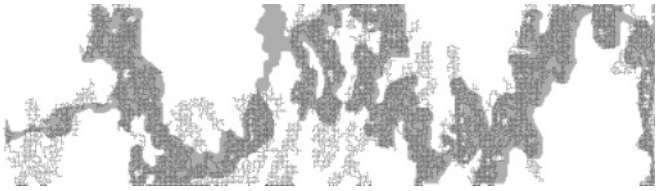

FIG. 7. As in Fig. 1 the occupation of air in the experimental cell is shown by the solid gray flow pattern. The air occupation from the efficient IPwt modeling is shown by the black pixels.

modeling results in closer agreement with experiment. In the papers of Glass and co-workers, the interfacial capillary pressure included not only the curvature due to the aperture spacing, of "radius r_1," between the top and bottom surfaces of the fracture but also an in-plane contribution due to an average curvature, of the local interface with "radius r_2" [6,9]. Consistent with invasion percolation models the potential invasion site with the smallest total capillary pressure is invaded by the nonwetting fluid. The references specify that an "arithmetic average of unit vectors to the right and left of the potential invasion site defines the local average fluid interface" (see Fig. 2 of Ref. [9]). The references also state that "in practice the number of sites on either side should not be less than five" [9]. Therefore, the in-plane curvature at the potential invasion site is represented by an arithmetic average over ten nearby sites on the interface, which smoothes the actual in-plane variations of the interface (see Fig. 2 of Ref. [9]). Results from this MIP show the expected smoothing of the interface, resulting in improved agreement between the efficient invasion percolation modeling approach and experiments. As mentioned earlier, like Karpyn and Piri, they compared the results from experimental flows in a "real fracture" with the coarser-scale numerical model of a similarly constructed real fracture with the aperture field being determined by optical methods [6]. Again, the modeling and experiment show similar structures, which may be the most one can expect in this case where the modeling and experiment were done for statistically similar but different fractures.

Even though the process of averaging over five sites to the right and to the left of the site to be advanced arbitrarily smoothes the local curvature, this MIP does appear to give good results for the two-phase flow using the same interfacial tension for both the in-plane and out-of-plane (i.e., aperture) curvatures.

We have developed a similar modification of IPwt, which emphasizes the short-range curvature. For example consider the three patterns in Fig. 8, showing a possible to-be-invaded voxel (gray) and its eight neighboring voxels.

The discretized "local curvature" is the difference between the slopes of the white lines. In (a) the change in local curvature is assigned a value $C = -2$ because occupation of the gray block reduces the magnitude of the curvature from 4 to 2, thereby reducing the effective capillary pressure. In (b) the

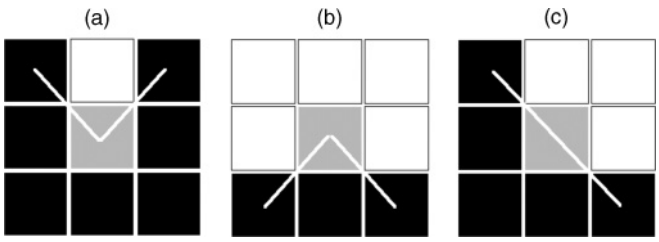

FIG. 8. Three of the 41 "short-range curvature patterns" (very local). In this figure, the black covering squares have already been invaded and the white covering squares are un-invaded. The gray covering square is on the interface that will be invaded, if its total capillary pressure [Eq. (2)] is the smallest on the whole interface. The white lines connect the "to-be-invaded" gray square to adjacent interface sites.

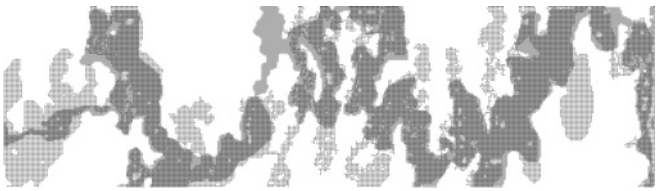

FIG. 9. Black pixels show the covering squares occupied by air. For this figure the curvature coefficient is $\alpha = 0.1$. This "best" value was determined from a trial and error visual comparison of our MIPwt flow pattern with the experimental flow pattern.

change in local curvature is assigned a value $C = +2$ because occupation of the gray block changes the magnitude of the curvature from 0 to $|-2|$ thereby increasing the effective capillary pressure. In (c) the change in local curvature is assigned a value $C = -2$ because occupation of the gray block decreases the magnitude of the curvature from 2 to $+0$, thereby decreasing the effective capillary pressure. For a few of the 41 short-range curvature patterns, it can be difficult to determine the exact "change-in-curvature" assignments; but we have tried to adhere to a scheme where values less than zero reduce the curvature of the interface and the total capillary pressure, while a positive value increases the curvature and capillary pressure.

This change in curvature C is added to the capillary pressure due to the apertures w so that the effective capillary pressure for one of the gray squares is given by the formula

$$P_c = \sigma \left(\frac{1}{w} + \alpha C \right), \tag{2}$$

where α is an adjustable parameter, which is the same for all 41 curvature patterns. As Fig. 9 illustrates, this simple modified invasion percolation does indeed make the invasion more compact, that is, much less ramified than the pattern from IPwt shown in Fig. 8.

Just as the averaging procedure of Glass and co-workers [6,9] reduces the role of the in-plane, interfacial curvature, the small value of the curvature coefficient α reduces the role of the large values of the short-range curvature used in this modeling. A significantly larger value of this curvature coefficient would overwhelm the effect of the apertures and make the pattern plug-like.

2. *Including the role of viscosity differences*

Since air is injected into a water-saturated model of a fracture in the experiment that we are attempting to model, viscosity effects should not be negligible for this small a viscosity ratio $M = \mu_{\text{air}}/\mu_{\text{water}}$. To approximate the effect of this small viscosity ratio, we have used the standard method of invasion percolation with a gradient in the capillary pressure,

$$P_c(x) = (1 - \beta x) P_c, \tag{3}$$

where P_c is given in Eq. (2) and x is in units of covering squares [29–31]. In this case, the gradient in capillary pressure is negative thereby decreasing the capillary pressure with distance x from the inlet. This decrease in capillary pressure with x is intended to account for the increased pressure gradient between the outlet and any air which is at distance x from the inlet. This increased pressure gradient results from the nearly constant pressure in the low viscosity air.

FIG. 10. Again voxel sized black dots show the air occupation from modeling.

For Fig. 10 the values used for the fitting coefficients in Eqs. (2) and (3) are $\alpha = 0.1$ and $\beta = 0.0018$. These values resulted from a trial and error visual comparison of our gradient modified MIPwt flow pattern with the experimental flow pattern. After these values had been chosen, we checked the saturation of the modeling result in Fig. 10 and found a value of 54.0% air saturation. This is in excellent agreement with the 53.5% saturation from experiment. It should be noted that the modeling patterns are not very sensitive to these values. For the values $\alpha = 0.2$ and $\beta = 0.0018$, extra fingers in the pattern center and outlet were slightly larger, giving a saturation of 56.5% so that a doubling of α changes the saturation by less than 5%. For $\alpha = 0.1$ and $\beta = 0.0016$, the finger at the outlet was slightly larger giving a saturation of 55% so that a change in β of more than 10% changes the saturation by less than 2%.

Using the same values of the curvature coefficient, $\alpha = 0.10$ and the gradient coefficient $\beta = 0.0018$, we also modeled the injection of air into the opposite side of the water-saturated flow cell. For this opposite direction the details of the air advance will be different because for the two different directions the air encounters a different sequence of covering square "choices" as it advances through the cell.

With no change in the parameters, the agreement of the modeling and experiment in Fig. 11 is nearly as good as the agreement in Fig. 10.

Although there are real differences between the modeling and experimental results, there is better overall agreement in the occupations than is seen in previous comparisons of modeling and experiment. It is likely that at least part of the disagreement between modeling and experiment observed in Figs. 10 and 11 is due to the errors of 3% or less in the apertures of the experimental flow model. These invasion percolation models are very sensitive to small changes in the capillary pressures. As a test of this sensitivity, we randomly assigned changes between $\pm 3\%$ to the apertures in the computer model; this resulted in a few moderate changes in the occupation, that is, different random number seeds resulted in changes of less

FIG. 11. Here the flow cell has been flipped (left-to-right) so that the air is injected (from the right) into what was the outlet in Fig. 10.

than 30% in one or two of the specific features of the modeling patterns in that certain of the smaller fingers in the modeling would appear smaller or larger with these randomly assigned changes. In spite of obvious unphysical aspects of the modeling like the crude approximation to the in-plane interfacial smoothing, the neglect of the sharp transition in aperture size between one block and the next and the very approximate treatment of viscous effects, the modeling gives surprisingly good detailed agreement with experiment, for a flow cell which is as close as possible to the fracture model used in the modeling.

IV. CONCLUSIONS

In developing accurate theory-based procedures for modeling two-phase flow through fractures, it is necessary to be able to compare computational results for a fracture with experiments performed on the exact same fracture. Previous comparisons of modeling and experiment have compared experiments performed on a real fracture with modeling that used a lower resolution mathematical model of that fracture [6–13]. These comparisons showed good qualitative agreement, but there were significant differences between modeling and experiment in the detailed fluid occupations. In this paper we present the first comparison of modeling with experiments performed on a physical fracture which is as nearly identical as possible to the virtual fracture used in the modeling, that is, with manufacturing experimental errors of less than 3% in the aperture values. In addition, this model includes an approximate treatment of viscosity differences for comparison with the experiments of air injection into a water-saturated flow cell. It should be noted that this unstable viscosity ratio is similar to that for injection of CO_2 into a brine-saturated fracture at high pressures. This important case of an unstable viscosity ratio does not seem to have been addressed in the previous modeling studies.

The flow patterns from our modeling that approximately includes both the effect of interfacial tension in smoothing the interface and the effect of viscosity ratio show good detailed agreement with the experimental flow patterns. This is especially true for the major features of the torturous flow paths. There are relatively minor differences which may be due in part to the manufacturing errors in aperture sizes of the experimental model and in part to approximations in the modeling procedures. In any case, a review of the literature shows that the detailed comparison of the flow patterns from experiment and modeling from earlier work is not as good as seen in Figs. 10 and 11. This suggests that differences seen in earlier work may be largely due to the currently unavoidable use of lower resolution mathematical models of the fracture in the modeling. Our direct comparison of modeling and experiment for essentially identical fractures shows that all of the different modeling schemes capture the general form of the flow, but that including the smoothing effects of in-plane interfacial tension significantly improves the agreement.

All of this suggests future work including a detailed study of how single-phase and two-phase flow are affected by tortuosity. Furthermore, it would obviously be useful to determine if there was a scale-coarsening cutoff at which the flow and tortuosity are only minimally different from the flow and tortuosity in the real fracture. It would also be useful if the surface tension smoothing of the interface were included in standard pore-level models.

ACKNOWLEDGMENTS

This study was funded by the US Department of Energy, Office of Fossil Energy. M. Ferer and G. Ahmadi gratefully acknowledge support of the US, DOE Office of Fossil Energy through the ORISE Faculty Research Participation Program. D. Crandall thanks the National Research Council and The National Energy Technology Laboratory for partial support. We appreciate the invaluable assistance of Douglas Leonard in constructing the experimental fracture flow cell.

[1] National Research Council, Committee on Fracture Characterization and Fluid Flow, Rock Fractures and Fluid Flow: Contemporary Understanding and Applications (National Academy Press, Washington, DC, 1996).
[2] L. J. Pyrak-Nolte *et al.*, *in Rock Joints*, edited by B. A. Stephansson (Balkema, Rotterdam, 1990), p. 405.
[3] Y. W. Tsang, Water Resour. Res. **20**, 1209 (1984).
[4] S. R. Brown, J. Geophys. Res. **94**, 9429 (1989).
[5] D. Crandall, G. Bromhal, and Z. T. Karpyn, Int. J. Rock Mechan. Mining Sci. **47**, 784 (2010).
[6] R. J. Glass, M. J. Nicholl, and L. Yarrington, Water Resour. Res. **34**, 3215 (1998).
[7] R. G. Hughes and M. J. Blunt, Adv. Water Res. **24**, 409 (2001).
[8] R. G. Hughes and M. J. Blunt, SPE J. **71297**, 126 (2001).
[9] R. J. Glass, H. Rajaram, and R. L. Detwiler, Phys. Rev. E **68**, 061110 (2003).
[10] M. Prodanović and S. L. Bryant, *Physics-Driven Interface Modeling for Drainage and Imbibition*, in 2007 SPE Annual Technical Conference and Exhibition, Anaheim, California.
[11] Z. T. Karpyn and M. Piri, Phys. Rev. E **76**, 016315 (2007).
[12] M. Piri and Z. T. Karpyn, Phys. Rev. E **76**, 016316 (2007).
[13] T. Petchsingto and Z. T. Karpyn, Hydrogeol. J. **18**, 1583 (2010).
[14] A. A. Keller, Int. J. Rock Mechan. Mining Sci. **34**, 155.e1 (1997).
[15] I. Kim, W. B. Lindquist, and W. B. Durham, Phys. Rev. E **67**, 046708 (2003).
[16] Z. T. Karpyn, A. S. Grader, and P. M. Halleck, J. Colloid Interface Sci. **307**, 181 (2007).
[17] R. L. Detwiler, H. Rajaram, and R. J. Glass, Phys. Rev. E **71**, 031114 (2005).
[18] M. Ferer *et al.*, Transport Porous Media **86**, 273 (2011).
[19] D. Crandall, G. Ahmadi, and D. H. Smith. *Modeling of Gas-Liquid Flow Through an Inter-connected Channel Matrix*, in ASME 2009 Fluids Engineering Division Summer Meeting, Vail, CO.
[20] D. Crandall, Thesis, Clarkson University, Potsdam, NY, 2007; FEDSM2009-78138.
[21] M. Ferer, G. S. Bromhal, and D. H. Smith, Phys. Rev. E. **76**, 046304 (2007).

[22] F. M. White, *Fluid Mechanics*, 7th ed. (McGraw-Hill, New York, 2010).
[23] M. Blunt and P. King, Phys. Rev. A **42**, 4780 (1990).
[24] E. Aker *et al*., Transport Porous Media **32**, 163 (1998).
[25] M. Ferer, G. S. Bromhal, and D. H. Smith, Physica A **319**, 11 (2003).
[26] M. Ferer, G. S. Brohmal, and D. H. Smith, Phys. Rev. E. **67**, 051601 (2003).
[27] M. Ferer *et al*., Phys. Rev. E **70**, 016303 (2004).
[28] P. Meakin, *Fractals, Scaling and Growth Far From Equilibrium* (Cambridge University Press, Cambridge, 1998).
[29] Y. C. Yortsos, B. Xu, and D. Salin, Phys. Rev. Lett. **79**, 4581 (1997).
[30] B. Xu, Y. C. Yortsos, and D. Salin, Phys. Rev. E **57**, 739 (1998).
[31] C.-H. Lam, Phys. Rev. Lett. **92**, 254503 (2004).